Journal of Materials and Environmental Sciences
ISSN : 2028-2508

JMES, 2017 Volume 8, Issue 5, Page 1708-1717

http://www.jmaterenvironsci.com/

An enhanced finite volume method for numerical simulation of turbulent shallow water flows

A. Abakouy[1], EM. Chaabelasri[1, 2], N. Salhi [1], I. Elmahi[3]

1. LME, Faculté des Sciences, BP. 717, 60000 Oujda, Maroc
2. Ecole National des Sciences Appliquées, BP.03, Ajdir Al-Hoceima
3. ENSAO, EMSN, COSTE, Université Mohammed 1, B.P. 669, 60000 Oujda, Morocco.

Received 29 Dec 2016,
Revised 21 Feb 2017,
Accepted 23 Feb 2017

Keywords
- ✓ Shallow water equations;
- ✓ Turbulence model;
- ✓ Depth-averaged $k-\varepsilon$ model;
- ✓ Finite volume;
- ✓ Unstructured mesh ;

A Abakouy
abkouy2012@gmail.com
+212635442905

Abstract

We consider in this work an expanded finite volume numerical approximation of the turbulent $k-\varepsilon$ shallow water equations, on unstructured meshes, we use a simple discretization in wish only physical fluxes and averaged states are used in their formulations. To control the local diffusion in the scheme and also to preserve monotonicity, a parameter is introduced based on the sign matrix of the flux Jacobian. Numerical results are presented and compared with experimental data, for a backward-facing flow problem, to demonstrate and confirm its capability to provide accurate simulation of turbulent flows. Furthermore, we test the method on a practical problem by simulating flows in Moulouya River. The main focus is to examine the performance of the method for complex geometries that involve water recirculation. The obtained results demonstrate its ability to capture the main flow features.

1. Introduction

Two-dimensional depth averaged models have become very popular since the last decades, and the shallow water equations in depth-averaged form have been successfully applied to many engineering problems, and their application fields include a wide spectrum of phenomena other than water waves. For instance, the shallow water equations have applications in environmental and hydraulic engineering such as tidal flows in an estuary or coastal regions, rivers, reservoir, and open channel flows. Such practical flow problems are not trivial to simulate because the geometry can be complex, and the topography tends to be irregular. In addition, most of water free-surface flows encountered in engineering practice are turbulent characterized. This property makes direct numerical simulation of turbulent flows very difficult.

In this paper, we adopt the depth-averaged $k-\varepsilon$ model proposed in [1], which was the first depth-averaged two-equation eddy viscosity model, and it is still the most commonly used with the depth-averaged models when turbulent effects are accounted for in the computation. The depth-averaged $k-\varepsilon$ model constitutes an alternative for direct numerical simulation and large eddy simulation in industrial codes. Their advantage lies in the fact that the resolved quantities are assumed to be deterministic and therefore require no effective capture of random fluctuations, especially in the near-wall regions. As a direct consequence, the spatial discretizations involved may be significantly more larges. More details concerning the depth-averaged models can be found in the references [2-3] and for research studies on modeling and numerical simulation of turbulent shallow water flows, we cite, for example, [4-5].

Research on numerical methods for the solution of the shallow water equations has attracted tremendous attention in the past years. The finite volume numerical discretization of the convective flux in the shallow water equations has been extensively studied in many recent works, see for example, [6-11]. A useful finite volume Non-Homogeneous Riemann Solver method in computing such solutions is proposed and studied throughout many papers by Benkhaldoun et al, in [12-14-16]. The flux gradient and source term are balancing and the

stability analysis of the scheme leads to the introduction of the sign matrix of the flux jacobian. The method is successfully applied in many problems and confirms its capability to provide accurate and efficient simulations of real problems, such the numerical simulation of pollution dispersion in the Strait of Gibraltar [15] and sediment transport in the Nador lagoon [17].
In the current work, we propose an enhanced finite volume method that incorporates the techniques of the methods proposed in [13]. Our main goal is to present a class of efficient numerical methods that can accurately solves the turbulent $k-\varepsilon$ shallow water equations. We, firstly, rearranged the turbulent $k-\varepsilon$ shallow water equations in a model forms a hyperbolic system of conservation laws with source terms. Then, the finite volume Non-Homogeneous Riemann Solver is used to solve this system. The method employs only physical fluxes and averaged states in their formulations. To control the local diffusion in the scheme and also to preserve monotonicity, a parameter is introduced based on the sign matrix of the flux Jacobian.
The structure of this paper is as follows. In Section 2, we present the mathematical equations for turbulent $k-\varepsilon$ shallow water equations. The formulation of the finite volume method is detailed in Section 3. Section 4 is devoted to numerical results. Finally, Section 5 contains the conclusions.

2. The turbulence shallow water equations

In conservation form, the two-dimensional non-linear shallow water equations are given by the depth-averaged continuity equation and the respective x- and y-depth-averaged momentum equations [18-19]:

$$\frac{\partial h}{\partial t}+\frac{\partial (hu)}{\partial x}+\frac{\partial (hv)}{\partial y}=0 \tag{1}$$

$$\begin{aligned}\frac{\partial (hu)}{\partial t}+\frac{\partial (hu^2+\frac{gh^2}{2})}{\partial x}+\frac{\partial (huv)}{\partial y}=&-gh\frac{\partial z_b}{\partial x}-\frac{S_{fx}}{\rho}+\frac{\partial}{\partial x}\left[(\upsilon+2\upsilon_t)\frac{\partial (hu)}{\partial x}\right]\\&+\frac{\partial}{\partial y}\left[(\upsilon+\upsilon_t)\left(\frac{\partial (hu)}{\partial y}+\frac{\partial (hv)}{\partial x}\right)\right]\end{aligned} \tag{2}$$

$$\begin{aligned}\frac{\partial (hv)}{\partial t}+\frac{\partial (huv)}{\partial x}+\frac{\partial (hv^2+\frac{gh^2}{2})}{\partial y}=&-gh\frac{\partial z_b}{\partial y}-\frac{S_{fy}}{\rho}+\frac{\partial}{\partial x}\left[(\upsilon+\upsilon_t)\left(\frac{\partial (hu)}{\partial y}+\frac{\partial (hv)}{\partial x}\right)\right]\\&+\frac{\partial}{\partial y}\left[(\upsilon+2\upsilon_t)\frac{\partial (hv)}{\partial y}\right]\end{aligned} \tag{3}$$

where h is the total depth from the sea bed to the free surface, u and v are the depth-averaged velocity components in the Cartesian x and y directions, z_b is the bed elevation above a fixed horizontal datum, g the acceleration due to gravity, and S_{fx} and S_{fy} are the bed shear stress components, defined as

$$S_{fx}=\rho C_b u\sqrt{u^2+v^2},\ S_{fy}=\rho C_b v\sqrt{u^2+v^2} \tag{4}$$

where ρ is the water density and C_b is the bed friction coefficient, which may be estimated from $C_b=\frac{gn_{\mathrm{M}}^2}{h^{1/3}}$, where n_{M} is the Manning coefficient, υ is the kinematic viscosity of water, and υ_t is a turbulent eddy viscosity, that quantify the energy dissipation due to the turbulent interactions among the particles.

To determine the turbulent eddy viscosity, the $k-\varepsilon$ model is used, in which k is the turbulence kinetic energy and ε is the dissipation rate per unit mass. The shallow water equations are obtained from depth integration, therefore it seems reasonable to use the same calcul of the $k-\varepsilon$ model [6]. Therefore, the turbulent eddy viscosity is calculated as:

$$\nu_t=C_\mu\frac{k^2}{\varepsilon} \tag{5}$$

Where k and ε are given by the transport equations

$$\frac{\partial(h\zeta)}{\partial t}+\frac{\partial(hu\zeta)}{\partial x}+\frac{\partial(hv\zeta)}{\partial y}=\frac{\partial}{\partial x}\left[(\upsilon+\frac{\upsilon_t}{\sigma_\zeta})h\frac{\partial\zeta}{\partial x}\right]+\frac{\partial}{\partial y}\left[(\upsilon+\frac{\upsilon_t}{\sigma_\zeta})h\frac{\partial\zeta}{\partial y}\right]+S_\zeta,\quad \zeta=(k,\varepsilon) \tag{6}$$

Where

$$\begin{cases} S_k=h\left[P_H+P_{kV}-\varepsilon\right] \\ S_\varepsilon=h\left[C_{\varepsilon1}\frac{\varepsilon}{k}P_H+P_{\varepsilon V}-C_{\varepsilon2}\frac{\varepsilon^2}{k}\right] \end{cases} \tag{7}$$

With

$$P_H=2\nu_t\left[\left(\frac{\partial u}{\partial x}\right)^2+\frac{1}{2}\left(\frac{\partial u}{\partial y}+\frac{\partial u}{\partial x}\right)^2+\left(\frac{\partial v}{\partial y}\right)^2\right],\ P_{kV}=\frac{1}{\sqrt{C_f}}\frac{U^{*3}}{h}\ \text{and}\ P_{\varepsilon V}=3,6\frac{C_{\varepsilon2}\sqrt{C_\mu}}{C_f^{3/4}}\frac{U^{*4}}{h^2}$$

P_H is the production of k due to interactions of turbulent stresses with horizontal mean velocity gradients, and P_{kV} and $P_{\varepsilon V}$ are the productions of k and ε due to vertical velocity gradients and are related to the friction velocity U^*. The friction coefficient C_f can be obtained as:

$$U^*=\sqrt{C\mu\frac{k^2}{\varepsilon}\left|\partial U\right|)} \tag{8}$$

Finally, the values of the empirical constants considered in this study are $C_\mu=0.09$, $C_{\varepsilon1}=1.44$, $C_{\varepsilon2}=1.92$, $\sigma_k=1.2$ and $\sigma_\varepsilon=1.3$.

3. Enhanced finite volume Scheme

For simplify, using matrix-vector notation, the two dimensional turbulent shallow water system can be written:

$$\mathbf{W}_t+\mathbf{F}_1(\mathbf{W})_x+\mathbf{F}_2(\mathbf{W})_y-\tilde{\mathbf{F}}_1(\mathbf{W})_x-\tilde{\mathbf{F}}_2(\mathbf{W})_y=\mathbf{S}(\mathbf{W}) \tag{9}$$

where W is the vector of dependent variables, $\mathbf{F}_1$, $\mathbf{F}_2$ are the inviscid flux vectors, $\tilde{\mathbf{F}}_1$, $\tilde{\mathbf{F}}_2$ are diffusive flux vectors, S is the vector of source terms, and the subscripts x, y, and t denote partial differentiation. In full, the vectors are:

$$\mathbf{W}=\begin{pmatrix} h \\ hu \\ hv \\ hk \\ h\varepsilon \end{pmatrix},\ \mathbf{F}_1=\begin{pmatrix} hu \\ hu^2+\frac{gh^2}{2} \\ huv \\ huk \\ hu\varepsilon \end{pmatrix},\ \mathbf{F}_2=\begin{pmatrix} hv \\ huv \\ hv^2+\frac{gh^2}{2} \\ hvk \\ hv\varepsilon \end{pmatrix},\ \tilde{\mathbf{F}}_1=\begin{pmatrix} 0 \\ (\upsilon+2\upsilon_t)\frac{\partial(hu)}{\partial x} \\ (\upsilon+\upsilon_t)(\frac{\partial(hu)}{\partial y}+\frac{\partial(hv)}{\partial x}) \\ (\upsilon+\frac{\upsilon_t}{\sigma_k})h\frac{\partial k}{\partial x} \\ (\upsilon+\frac{\upsilon_t}{\sigma\varepsilon})h\frac{\partial\varepsilon}{\partial x} \end{pmatrix},$$

$$\tilde{\mathbf{F}}_2 = \begin{pmatrix} 0 \\ (\upsilon+\upsilon_t)(\frac{\partial(hu)}{\partial y}+\frac{\partial(hv)}{\partial x}) \\ (\upsilon+2\upsilon_t)\frac{\partial(hv)}{\partial y} \\ (\upsilon+\frac{\upsilon_t}{\sigma_k})h\frac{\partial k}{\partial y} \\ (\upsilon+\frac{\upsilon_t}{\sigma_\varepsilon})h\frac{\partial \varepsilon}{\partial y} \end{pmatrix} \text{ and } \mathbf{S} = \mathbf{S}_1 + \mathbf{S}_2 = \begin{pmatrix} 0 \\ -gh\frac{\partial Zb}{\partial x} \\ -gh\frac{\partial Zb}{\partial y} \\ 0 \\ 0 \end{pmatrix} + \begin{pmatrix} 0 \\ -ghS_{fx} \\ -ghS_{fy} \\ S_k \\ S_\varepsilon \end{pmatrix} \tag{10}$$

In order to discretize system (9), the domain is meshed with a set of conforming triangular elements. Using the control volume dedicted in Figure 1, a finite volume discretization of (9) yields

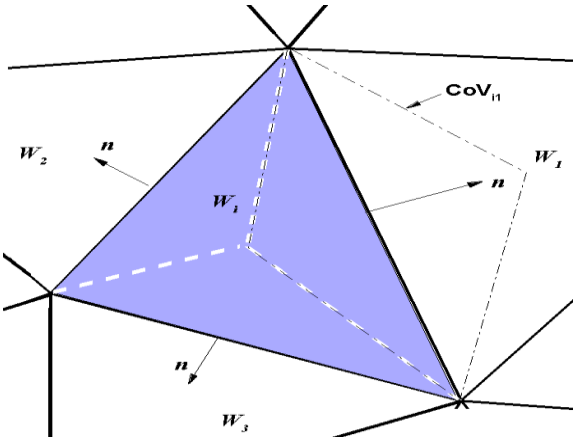

Figure 1: Control volume model and notations.

$$\frac{(\mathbf{W}_i^{n+1}-\mathbf{W}_i^{n})}{\Delta t}|V_i| + \sum_{j\in N(i)}\int_{\Gamma_{ij}} \mathbf{F}(\mathbf{W}^n,\hat{\mathbf{n}})\,d\Gamma - \sum_{j\in N(i)}\int_{\Gamma_{ij}} \tilde{\mathbf{F}}(\mathbf{W}^n,\hat{\mathbf{n}})\,d\Gamma = \int_{V_i} \mathbf{S}(\mathbf{W}^n)\,dV \tag{11}$$

Where $\mathbf{W}_i^{\,n} = \mathbf{W}(x_i,t_n)$ is the vector of conserved variables evaluated at time level $t_n = n\Delta t$, n is the number of time steps, Δt is the time step, and $|V_i|$ is the area of cell V_i. F and $\hat{F}$ are the advection and diffusion fluxes given by

$$\begin{aligned} \mathbf{F}(\mathbf{W}^n,\hat{\mathbf{n}}) &= \mathbf{F}_1(\mathbf{W}^n,\hat{\mathbf{n}}) + \tilde{\mathbf{F}}_1(\mathbf{W}^n,\hat{\mathbf{n}}) \\ \tilde{\mathbf{F}}(\mathbf{W}^n,\hat{\mathbf{n}}) &= \mathbf{F}_2(\mathbf{W}^n,\hat{\mathbf{n}}) + \tilde{\mathbf{F}}_2(\mathbf{W}^n,\hat{\mathbf{n}}) \end{aligned} \tag{12}$$

To evaluate the state $\mathbf{W}_i^n$, an approximation is required of the convective and diffusive flux terms at each edge of the cell. For this purpose, a Non Homogeneous Riemann Solver, developed in [12-14] for non-homogeneous hyperbolic systems to evaluate the convective flux. In this work, a special attention was taken to extend this scheme to $k-\varepsilon$ turbulent shallow water flows. The construction of the numerical scheme is based on the hyperbolicity of the system and the self-similarity of the solution, it's consists of a predictor and corrector stages as:

$$\boldsymbol{W}_{ij}^n = \tfrac{1}{2}(\boldsymbol{W}_i + \boldsymbol{W}_j) - \tfrac{1}{2}\mathrm{sgn}\left[\boldsymbol{A}(F(\overline{\boldsymbol{W}_{ij}^n},\boldsymbol{n}))\right](\boldsymbol{W}_j^n - \boldsymbol{W}_i^n) + \tfrac{1}{2}\left[\boldsymbol{A}(F(\overline{\boldsymbol{W}_{ij}^n},\boldsymbol{n}))^{-1}\right]\boldsymbol{S}_{ij} \tag{13}$$

$$\frac{(\mathbf{W}_i^{n+1}-\mathbf{W}_i^{n})}{\Delta t}|V_i| = \sum_{j\in N(i)}\int_{\Gamma_{ij}} \mathbf{F}(\mathbf{W}^n,\hat{\mathbf{n}})\,d\Gamma = \int_{V_i} \mathbf{S}(\mathbf{W}^n)\,dV \tag{14}$$

Where $\boldsymbol{A}(F(\overline{\boldsymbol{W}_{ij}^{n}},\boldsymbol{n}))$ is the Jacobian matrix with respect to $\boldsymbol{W}_{ij}^{n}$, and $\overline{\boldsymbol{W}_{ij}^{n}}$ is approximated either by Roe's average state.

To determine the sign matrix of the Jacobian in the prediction stage, a projection of $k-\varepsilon$ turbulent shallow water equations (9) including only advection and slope terms according to the normal η and tangential τ is required. In condensed form the resulting projection can write as [15]:

$$U_t+\mathbf{F}_\eta(U)_x=\mathbf{S}_\eta(U) \tag{15}$$

Where

$$U=\begin{pmatrix} h\\ hu_\eta\\ hu_\tau\\ hk\\ h\varepsilon \end{pmatrix},\quad \mathbf{F}_\eta=\begin{pmatrix} hu_\eta\\ hu_\eta{}^2+\frac{gh^2}{2}\\ hu_\eta u_\tau\\ hu_\eta k\\ hu_\eta \varepsilon \end{pmatrix},\quad \mathbf{S}_\eta=\begin{pmatrix} 0\\ -gh\frac{\partial Zb}{\partial \eta}\\ 0\\ 0\\ 0 \end{pmatrix} \tag{16}$$

u_η and u_τ are the normal and tangential velocity. Then a upwind scheme is used for the evaluation of the projected averaged state U_{ij}^{n} on each adge Γ_{ij} . The predictor stage is then formulated as:

$$U_{ij}^{n}=\tfrac{1}{2}(U_i+U_j)-\tfrac{1}{2}\mathrm{sgn}\left[\boldsymbol{A}(F_\eta(\overline{U_{ij}^{n}},\boldsymbol{n}))\right](\boldsymbol{U}_j^{n}-\boldsymbol{U}_i^{n})+\tfrac{1}{2}\left[\boldsymbol{A}(F_\eta(\overline{U_{ij}^{n}},\boldsymbol{n}))^{-1}\right]\boldsymbol{S}_{ij} \tag{17}$$

Where U and F_η as some defined in (16), $\overline{U}$ is the Roe's average state and $\boldsymbol{S}_{ij}$ is the slope term vector upwinded given by:

$$U=\tfrac{1}{2}\left(h_i+h_j\right)\begin{pmatrix} 1\\ \frac{u_i\sqrt{h_i}+u_j\sqrt{h_j}}{\sqrt{h_i}+\sqrt{h_j}}\eta_x+\frac{v_i\sqrt{h_i}+v_j\sqrt{h_j}}{\sqrt{h_i}+\sqrt{h_j}}\eta_y\\ -\frac{u_i\sqrt{h_i}+u_j\sqrt{h_j}}{\sqrt{h_i}+\sqrt{h_j}}\eta_y+\frac{v_i\sqrt{h_i}+v_j\sqrt{h_j}}{\sqrt{h_i}+\sqrt{h_j}}\eta_x\\ \frac{k_i\sqrt{h_i}+k_j\sqrt{h_j}}{\sqrt{h_i}+\sqrt{h_j}}\\ \frac{\varepsilon_i\sqrt{h_i}+\varepsilon_j\sqrt{h_j}}{\sqrt{h_i}+\sqrt{h_j}} \end{pmatrix},\mathbf{S}_{ij}=-g\,\frac{h_i-h_j}{2}(Z_i-Z_j)\begin{pmatrix} 0\\ 1\\ 0\\ 0\\ 0 \end{pmatrix} \tag{18}$$

$\mathrm{sgn}\left[\boldsymbol{A}(F_\eta(\overline{U_{ij}^{n}},\boldsymbol{n}))\right]$ denotes the sign matrix of the Jacobian $\boldsymbol{A}(F_\eta(\overline{U_{ij}^{n}},\boldsymbol{n}))$, defined by:

$$\mathrm{sgn}\left[\boldsymbol{A}(F_\eta(\overline{U_{ij}^{n}},\boldsymbol{n}))\right]=\mathbf{R}(\overline{U})\,\mathrm{sgn}\left[\boldsymbol{\Lambda}(\overline{U})\right]\mathbf{R}(\overline{U})^{-1} \tag{19}$$

$$\left[\boldsymbol{A}(F_\eta(\overline{U_{ij}^{n}},\boldsymbol{n}))\right]=\mathbf{R}(\overline{U})\left|\boldsymbol{\Lambda}(\overline{U})\right|\mathbf{R}(\overline{U})^{-1} \tag{20}$$

$\mathbf{R}(\overline{U})$ and $\mathbf{\Lambda}(\overline{U})$ are respectively the eigenvector and eigenvalue matrices of $\boldsymbol{A}(F_\eta(\overline{U_{ij}^n}, \boldsymbol{n}))$. In [14] find out more details on the explicit form of the matrix in (10).

Once the the projected state U_{ij}^n on each edge Γ_{ij} is obtained using (17), the conservative state $\boldsymbol{W}_{ij}^n$ is then evaluated using the transformations $u = u_\eta n_x + u_\tau n_y$ and $v = v_\eta n_x + v_\tau n_y$ .To discretize the diffusion fluxes in (9) we used a Green-Gauss diamond reconstruction, adopted by [15-16]. This method is selected because is applied for unstructured triangular mesh without any restriction on the angles of triangles. The construction of the method begins by the reconstruction of a co-volume coV_{ij} centred on the edge Γ_{ij} by connecting barycentres of the triangles that share the edge Γ_{ij} and its endpoints. The diffusion flux at the interface Γ_{ij} is the evaluated as :

$$\int_{\Gamma_{ij}} (\nu + \nu_t) h \frac{\partial \psi}{\partial \xi} n_\xi d\Gamma = (\nu + \nu_t)|_{\Gamma_{ij}} \; h|_{\Gamma_{ij}} \; \frac{\partial \psi}{\partial \xi}|_{\Gamma_{ij}} \int_{\Gamma_{ij}} n_\xi d\Gamma \tag{21}$$

Where $\psi, \xi \; and \; n_\xi$ denote, respectivement $(u, v, k, \varepsilon), (x, y)$ and (n_x, n_y) in diffusion vector. The gradient $\frac{\partial \psi}{\partial \zeta}$ on the interface Γ_{ij} are computed using the nodes of the co-volume coV_{ij} (see figure 1) as follows:

$$\frac{\partial \psi}{\partial \xi}|_{\Gamma_{ij}} = \frac{1}{\left|CoV_{ij}\right|}|_{\Gamma_{ij}} \sum_{\varepsilon \in \partial CoV} \left(\frac{\psi_{N_1} + \psi_{N2}}{2} \int_\varepsilon n_{\xi\varepsilon} d\sigma \right) \tag{22}$$

Where N_1 and N_2 are the nodes of the edge ε on the surface ∂coV_{ij} , ψ_{N_1} and ψ_{N_2} are the values of the incnoune ψ in the node N_1 and N_2 , respectively.

4. Results and Discussion

For demonstrate the performance and accuracy of the developed scheme, two test cases are selected. The first example is a turbulent flow in a channel with forward-facing step for which experimental results are available. This example is selected to test the performance of the model to reproduce the experimental results, especially the recirculation zone after the expansion though a qualitative comparison of the numerical results to the experimental data. The second is a practical test example in a section of Moulouya River; the computational domain is a real domain contains complicated two-dimensional geometries, eddy viscosity; which can be a challenge for most numerical methods. In the examples reported in this work, the stability of the the present explicit scheme is guaranteed by choosing a time stepsize Δt according to the Courant-Friedrichs-Lewy (CFL) criterion, giving :

$$\Delta t = CFL \min_{\Gamma_{ij}} \left(\frac{|V_i| + |V_j|}{2|\Gamma_{ij}| \max(|(\lambda_p)_{ij}|)} \right) \tag{23}$$

where CFL is the Courant number ($0 < CFL < 1$), $(\lambda_p)_{ij}$ is the eigenvalue of the system evaluated at the interface Γ_{ij} between two cells V_i and V_j .For all numerical solutions presented here, the Courant number is set to $CFL = 0.6$ and the initial conditions are selected for the water depth as inlet boundary when the flow are at rest.

5. Flow in a channel with for forward-facing step

Two-dimensional turbulent flow past a sudden expansion in a sidewall is the first example, in order to test the ability of the numerical model to reproduce the recirculation zone that develops behind a step due to flow separation at a step. The results will be compared against data obtained by Fe et al. [20] who carried out an experimental and numerical study of recirculation in a water channel containing a sidewall expansion. The computational domain consists in a $0,5m \times 3,5m$ horizontal channel with an abrupt expansion located at $1m$ from the inlet, commonly known as backward facing step (show figure 2). The inflow discharge at the left boundary is enforced with $20.2l/s$ and imposed a water height of $24.2cm$ at the outflow boundary. the no-slip condition assumes that at a solid boundary, the fluid will have zero velocity is imposed for the rest. An unstructured triangular mesh are generated for the channel with consist of a 2000 nodes and 3691 elements (see figure 3).

In Figure 4 and 5, we present a comparison between experimental and computational results; we illustrate the snapshot of the velocity and the kinetic energy along with the velocity fields. For clear presentation, we have also included streamlines within the presented results. From these results, we can see that the proposed method resolves accurately the flow structures, and the vortices seem to be localized in the correct place in the flow domain. For instance, the recirculation zone is in good agreement with the experimental measurements. For more comparisons, Figure 6 shows profiles of the velocity at $x = 1.53m$ within the measurement values. A good agreement between measured and predicted profiles has been obtained.

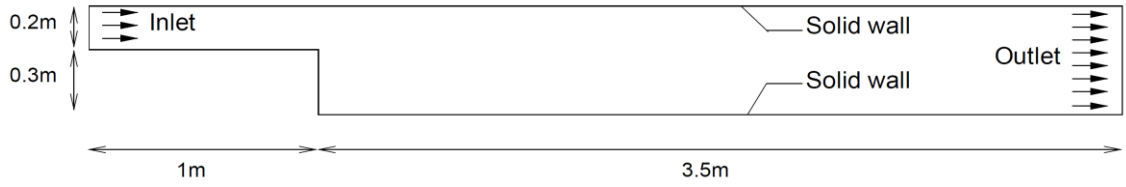

Figure 2: Flow in channel with a backward-facing step: Definition of problem domain.

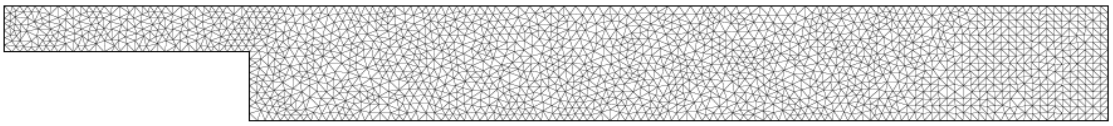

Figure 3: Flow in channel with a backward-facing step: Unstructured triangular mesh used in numerical model.

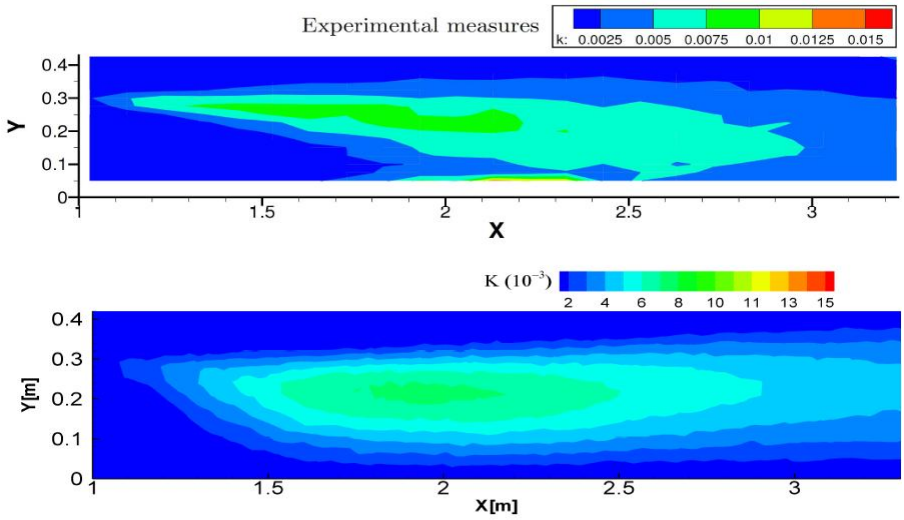

Figure 4: Flow in channel with a backward-facing step: Comparison of experimental (top) and numerical (bottom) results of kinetic energy k.

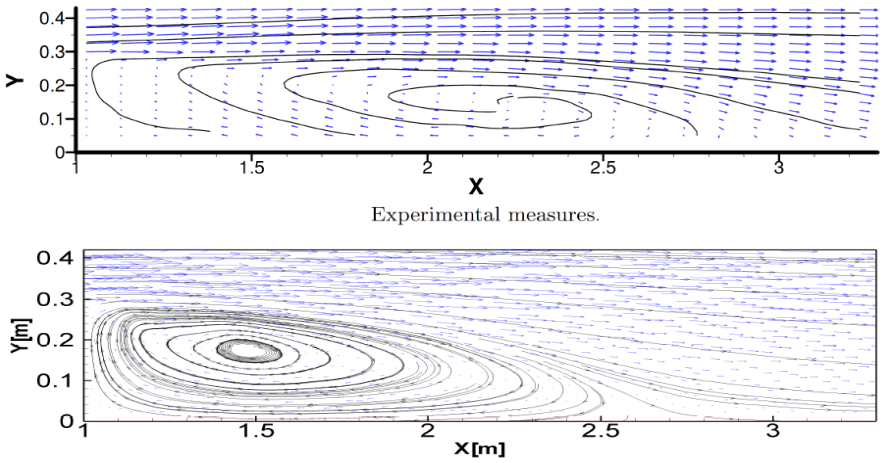

Figure 5: Flow in channel with a backward-facing step: Comparison of experimental (top) and numerical (bottom) results of velocity fields.

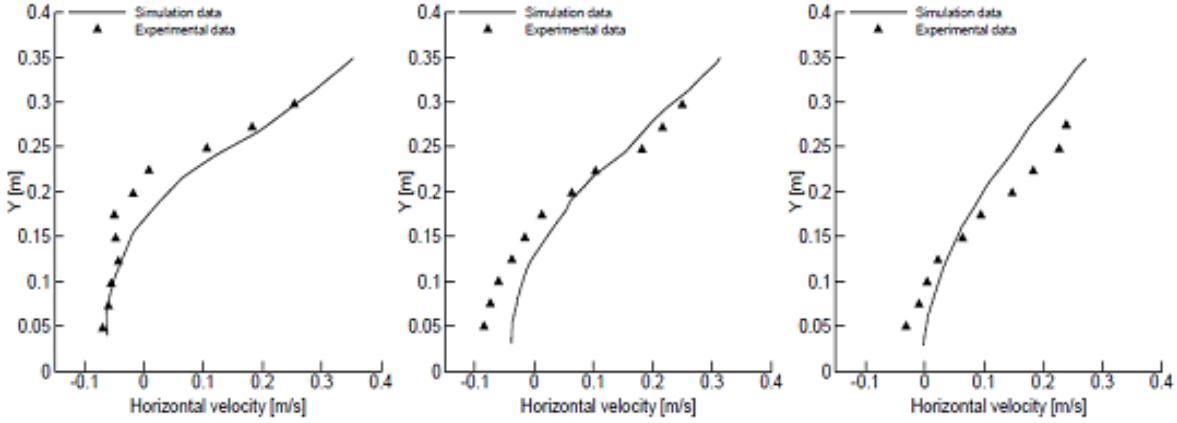

Figure 6: Flow in channel with a backward-facing step: a cross section at x=1.53m, 2.03m and 2.53m of the velocity, with a comparison between experimental and numerical results.

6. Turbulent shallow water flow in Moulouya River

The method proposed has been also applied to modeling steady turbulent flow in a small shallow river. The selected domain is one reach of the Moulouya River in Morocco, near Rass Elma City. Figure 7 displays the digital map of the selected domain, the total length of the calculated river reach is 280m, the flow direction if from the southwest to the northeast. A flow velocity 0.35m/s is set to at the inlet boundary, and the water depth is set to 1.5m at the outlet boundary, assuming that initially all computational cells in each of the streams had a velocity equal to zero. The river has small bathymetry irregularities with horizontal dimensions, no wetting drying case are considered herein. The Manning coefficient is set to 0.005. An unstructured triangular mesh are generated, which consists of 24350 nodes and 46921 elements (figure 8), to use for computations. A CFL=0.6 is used of computational runs.

The figure 9 shows the simulation results which represent the behaviours of flow throughout, respectively, velocity magnitude and streamlines. The figures 10 represents a zooming snapshot over the largest recirculation zone, it contains the distribution of velocity fields and turbulent kinetic energy. These results show that the turbulent flow in the curved river has common behaviour with the open channel flow with forward-facing step. There is the large recirculation region after the bend when the flow tends to move to the opposite bank. The irregularities of the river generate this structure of the flow throughout these shores. The model predictions are reasonable in terms of magnitude as well as general direction of the depth-averaged velocities and accurately reproduce a region of recirculation along the inner bank downstream of the bend.

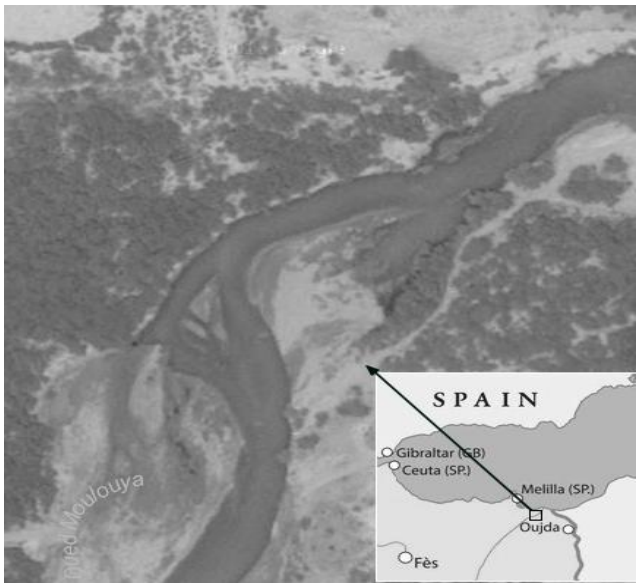

Figure 7: Turbulent shallow water flow in Moulouya River: Geographical map and location.

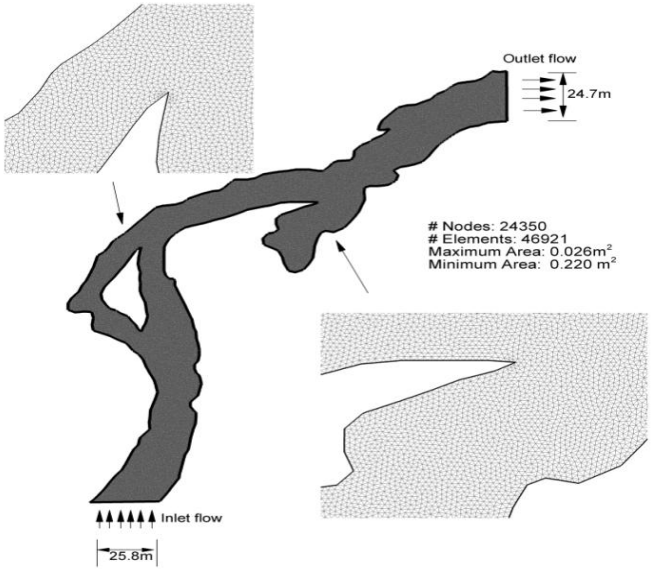

Figure 8: Turbulent shallow water flow in Moulouya River: Unstructured triangular mesh used in numerical model

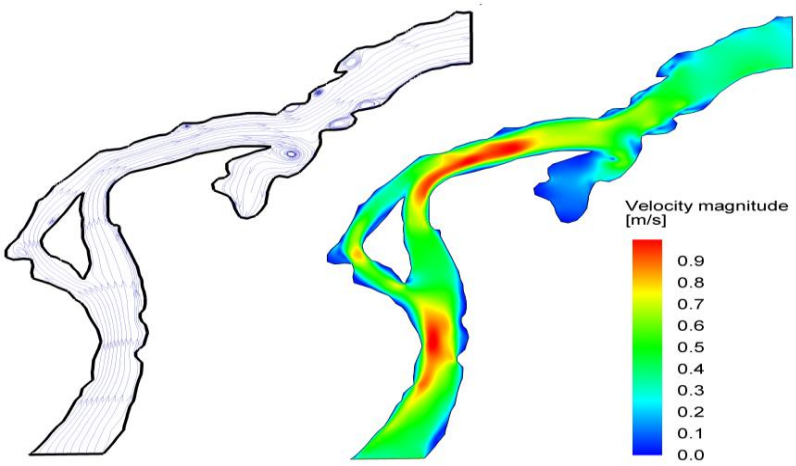

Figure 9: Turbulent shallow water flow in Moulouya River: streamlines and velocity magnitude.

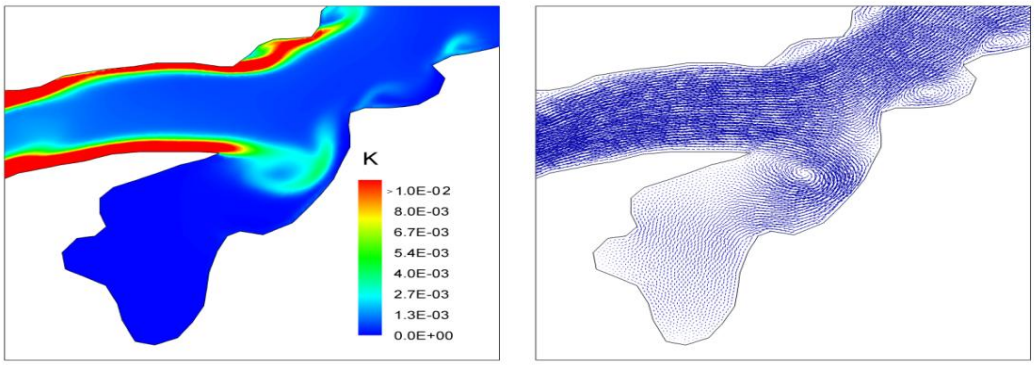

Figure 10: Turbulent shallow water flow in Moulouya River: Turbulent kinetic energy (left) and flow field (right).

Conclusions

In this study, a enhanced finite volume numerical approximation based on the Non-Homogeneous Riemann Solver formulation was expanded and applied to the turbulent shallow water problem. The governed equations are based on two dimensional depth-averaged model which combines the basic shallow water equations and depth-averaged $k-\varepsilon$ model. The numerical model was performed to investigate a turbulent open channel flow. Overall, through the turbulent flow simulations in backward-facing channel and Moulouya River, the results showed good agreement with experimental data, which implies the capability of the scheme in resolving accurately the flow structures. Furthermore, the model shows acceptable results in modeling turbulent flow in open channels, as well as tow-dimensional flow.

References

1. Rastogi AK., Rodi W., *ASCE. J. Hyd. Divi.*, 104 (1978) 397.
2. Pope S. B., Turbulent Flows, (2000), Cambridge University Press, *Book ISBN*: 0 521 59886 9.
3. Prud'homme M., Eléments-turbulence (2006) Published by Presses Internationales Polytechnique, Montreal, PQ, Canada *book ISBN* 10: 2553014074 / *ISBN* 13: 9782553014079.
4. Cea L., Puertas J., Vázquez-Cendón ME., *Arch. Comp. Meth. Eng.*, 14 (2007) 303.
5. Cea L., French JR., Vázquez-Cendón ME., *Int. J. Num. Meth. Eng.*, *67* (2006) 1909.
6. Duran A., Liang Q., Marche F., *J. Comp. Phys.*, 235 (2013) 565.
7. Berthon C., Marche F., *SIAM. J. Sci. Comp.*, 30 (2008) 2587.
8. Castro M., Gallardo J., López-GarcÍa J., Parés C., *SIAM J. Num. Anal.*, 46 (2008) 1012.
9. Chaabelasri E.M., Salhi N., Elmahi I., Benkhaldoun F., *Phys. & Chem. New.* 53 (2010) 119.
10. Gallardo J.M., Parés C., Castro M., *J. Comp. Phys.*, 227 (2007).
11. Gosse L., *J. Comp & Math. Appl.* 39 (2005) 135.
12. Benkhaldoun F., Elmahi I., Seaid M., *Comp. Meth. App. Mec. & Eng.* 199 (2010).
13. Sahmim S., Benkhaldoun F., Alcrudo F., *J. Comp. Phys.* 226 (2007) 1753.
14. Benkhaldoun F., Elmahi I., Seaïd M., *Math & Comp. Sim.*, 79 (2009).
15. Benkhaldoun F., Elmahi I., Seaid M., *J. Comp. Phys.* 226 (2007) 180.
16. Benkhaldoun F., Elmahi I., Seaid M, *Comp. Meth. Appl. Mec. & Eng.* 199 (2010) 3324.
17. Benkhaldoun F., Daoudi S., Elmahi I., Seaid M., *Appl. Num. Math.* 62 (2012) 1749.
18. Marche F., Etude théorique et numérique de modèles type Saint Venant. Application à l'hydrodynamique littorale. *PhD. Thèse Bordeaux, France* (2005).
19. Hervouet J. M., Hydrodynamics of Free Surface Flows: Modelling with the Finite Element Method (2007) *Book ISBN*: 978-0-470-31963-5
20. Navarrina J. Fe, F., Puertas J., Vellando P., Ruiz D., *Int. J. Num. Meth. & Flu.* 00 (2000) 1.